

SELF-SIMILAR CURRENT SHEET COLLAPSE TRIGGERED BY “IDEAL” TEARING

ANNA TENERANI
EPSS, UCLA, Los Angeles, CA

MARCO VELLI
EPSS, UCLA, Los Angeles, CA

ANTONIO FRANCO RAPPAZZO
Advanced Heliophysics, Pasadena, CA

FULVIA PUCCI
Università degli studi di Roma Tor Vergata, Rome, Italy
Draft version April 16, 2019

ABSTRACT

We study the onset and evolution of fast reconnection via the “ideal” tearing mode instability within a collapsing current sheet at high Lundquist numbers ($S \gg 10^4$). As the collapse proceeds, fast reconnection is triggered well before a Sweet-Parker type configuration can form: after the linear phase of the initial instability, X-points collapse and reform nonlinearly, a hierarchy of “ideal” tearing modes repeating faster and faster on current sheets at ever smaller scales. We present a simple model describing the self-similar evolution which explains both the timescale of the disruption of the initial sheet and the consequent turbulent spectra.

1. INTRODUCTION

Reconnection is thought to be the mechanism at the heart of many explosive processes observed in natural and laboratory plasmas, but how fast magnetic energy release is triggered in high Lundquist (S) and Reynolds (R) number plasmas has remained controversial. Recently, it has been shown that a tearing mode instability can grow on ideal timescales (“ideal” tearing, or IT) once a current sheet width becomes thin enough, or rather the inverse aspect ratio a/L reaches a scale $a/L \sim S^{-1/3}$ (Pucci & Velli 2014). The latter provides a natural, critical threshold for current sheets that can be formed before they disrupt over a few Alfvén times. For $S \rightarrow \infty$ this threshold inverse aspect ratio is much greater than that of the Sweet-Parker current sheet (SP), for which $a_{\text{SP}}/L \sim S^{-1/2}$, suggesting that a configuration *à la* Sweet-Parker should never be achieved when approaching the ideal limit, contrary to what is often thought (see, e.g., (Cassak & Drake 2013) and references therein). This is confirmed by the paradoxical nature of the reconnecting instability of the SP current sheet itself, the so called plasmoid instability, whose growth rate diverges with increasing S once Lundquist numbers become large enough, $S > 10^4$ (Loureiro et al. 2013).

At intermediate Lundquist numbers, say, $S \simeq 10^4 - 10^5$, the presence of inflow-outflows within a current sheet affects the scaling of the critical threshold for IT by inducing the formation of more elongated current sheets, that is, of layers having inverse aspect ratios $a/L \sim S^{-\alpha_c}$, with $\alpha_c > 1/3$ (Velli et al. 2015). Therefore, if the Lundquist number is not sufficiently large, the two descriptions –the IT instability on the

one hand, and the plasmoid instability on a SP sheet on the other– may be hard to distinguish. Nevertheless, the above arguments (see also Velli et al. (2015)) suggest that studying fast reconnection starting from an SP sheet or from a presumed SP born via the initial reconnection of a thicker, macroscopic sheet, while plausible for low S simulations, is incorrect when realistic Lundquist numbers $S \simeq 10^6 - 10^{14}$ are involved. Indeed, recent papers on the asymptotic tearing instability in thin current sheets (Pucci & Velli 2014; Tenerani et al. 2015; Del Sarto et al. 2015) have shown that the maximum growth rate increases nonlinearly with the aspect ratio (see also eq. (1) below) implying that the collapse to the critical threshold thickness may provide the trigger for fast reconnection.

Here we study the onset and evolution of the tearing instability within a single collapsing current sheet at $S = 10^6$. We show that (i) the transition to a fast tearing mode instability takes place when an inverse aspect ratio of the order of the threshold $a/L \sim S^{-1/3}$ is reached, and (ii) that the secondary current sheets forming nonlinearly –whose thickness, remarkably, scale as $\delta_i/L \sim S^{-1/2}$ – become the source of a cascade of super-Alfvénic reconnection events at increasingly faster rates. Such a cascade of fast tearing modes leads rapidly to a hierarchy of self similar structures which we model in a vein similar to that of the fractal reconnection scenario proposed by (Shibata & Tanuma 2001), modified by the scalings of the “ideal” tearing.

2. TRIGGER OF FAST RECONNECTION: SCENARIO

Let us consider a (local) Harris current sheet (cfr. eq. (2)) of inverse aspect ratio a/L , with Alfvén speed v_A and magnetic diffusivity η , in a high $S = Lv_A/\eta \gg 1$

plasma which is collapsing via some external process on a timescale $\tau_c \sim a (da/dt)^{-1}$, of the order of the ideal timescale, $\tau_c \gtrsim \tau_A = L/v_A$. We extend the linear analysis of the tearing instability to this time-dependent case by defining an instantaneous growth rate $\gamma(k, t)$, k being the wave number along the sheet, where explicit time-dependence is introduced by the evolving aspect ratio L/a itself.

In the static case, two regimes describe the unstable spectrum of a current sheet: the so called small Δ' regime, for wavelengths close to the instability threshold (or const.- ψ (Furth et al. 1963), for $ka \lesssim 1$ for the Harris sheet), and the large Δ' regime (or non const.- ψ (Coppi et al. 1976), for $ka \ll 1$). These two regimes lie respectively to the right and to the left of the fastest growing mode (Del Sarto et al. 2015; Loureiro et al. 2013), characterized by the following wave number and growth rate (Pucci & Velli 2014):

$$k_m a \sim S^{-1/4} (L/a)^{1/4}, \quad \gamma_m \tau_A \sim S^{-1/2} (L/a)^{3/2}. \quad (1)$$

Similarly to eqs. (1), the growth rates in the small and large Δ' regimes also increase with the aspect ratio; however, their values tend to zero in the asymptotic limit $S \rightarrow \infty$, and the full $\gamma(k)$ dispersion relation becomes rapidly peaked around k_m (cfr. Fig. 1 of (Pucci & Velli 2014)). Therefore, both the small and large Δ' regimes can be neglected in the framework of fast reconnection, since the development of the instability is controlled by the evolution of the fastest growing mode described by eqs. (1). Take the Harris sheet, for example: the unstable spectrum lies within the range $2\pi/L \lesssim k < 1/a$. From this condition and the first of eqs. (1) it follows that the regime described by eqs. (1) always exists once $k_m L \gtrsim 2\pi$, i.e. once $a/L \lesssim 0.2 S^{-1/5}$. The second of eqs. (1) shows that the growth rate becomes ideal when approaching the critical width $a/L \sim S^{-1/3}$ (much smaller than $S^{-1/5}$) from above. The transition to “ideal” tearing during collapse therefore occurs on the fastest growing mode, and not, as previously suggested, in a regime of wave numbers satisfying the small Δ' regime typical of thick sheets (Uzdensky & Loureiro 2014). In conclusion, a collapse with $\tau_c \gtrsim \tau_A$ naturally drives a sudden switch from a quasi-stable state –growth rate depending on a negative power of S – to an ideally unstable one.

We now consider the example of an exponential collapse, typically observed both in turbulence simulations (Biskamp 2000; Rappazzo & Parker 2013) and during the nonlinear stage of the classic tearing instability itself (see (Del Sarto et al. 2015) and references therein).

3. NUMERICAL SET UP

We consider a plasma with homogeneous density ρ_0 and pressure p_0 . The background magnetic field \mathbf{B}_0 describes an exponentially shrinking current sheet and is given by

$$\mathbf{B}_0 = B_0 \tanh [y/a(t)] \hat{\mathbf{x}} + B_0 \operatorname{sech} [y/a(t)] \hat{\mathbf{z}}, \quad (2)$$

where the half width $a(t)$ is prescribed and parametrized in time by

$$a(t) = a_0 \exp^{-t/\tau_c} + a_\infty (1 - \exp^{-t/\tau_c}). \quad (3)$$

Table 1

Simulation parameters: Lundquist number, collapsing time, asymptotic half width, onset time, nonlinear time, and half width reached at the end of the linear stage.

run #	S	τ_c/τ_A	a_∞/L	τ_*/τ_A	τ_{nl}/τ_A	$a(\tau_{nl})/L$
run 1		1	$S^{-1/3}$	3	16	0.01
run 2	10^6	4	$S^{-1/3}$	11.5	22	0.0105
run 3		10	$S^{-1/3}$	16	36	0.013
run 4		1	$S^{-1/2}$	3	4.5	0.0024

We employ a 2.5D compressible MHD code periodic in x and with non-reflecting boundary conditions along the inhomogeneous y direction (Landi et al. 2005). We assume an adiabatic closure, with index $\Gamma = 5/3$, a scalar resistivity, and a Newtonian viscous stress tensor with Prandtl number $P = 1$. With this choice, viscosity does not affect the scalings of IT significantly (Tenerani et al. 2015). The collapse of the background magnetic field is obtained by adding a forcing term \mathcal{F} of the form

$$\mathcal{F} = \left(\frac{1}{a} \frac{\partial a}{\partial t} \right) y \frac{\partial \mathbf{B}_0}{\partial y} \quad (4)$$

in Faraday’s equation. Magnetic and velocity fields are normalized to B_0 and to $v_A = B_0/\sqrt{4\pi\rho_0}$, respectively, lengths to the macroscopic length L , time to τ_A , and density and pressure to ρ_0 and $B_0^2/4\pi$, respectively. It is useful to introduce also the normalized flux function ψ , such that $\mathbf{B} = \nabla \times \psi \hat{\mathbf{z}}$. We set $p_0 = 0.8$ and $S = 10^6$. Instability is seeded with a random noise of small amplitude. Because of the wide range of scales to be resolved in the y direction, we employ an inhomogeneous grid with increasing resolution at the neutral line. The simulation box has normalized dimensions $L_x \times L_y = 2\pi \times 0.96$ (runs 1–3) and $L_x \times L_y = 2\pi \times 0.46$ (run 4), with 2048×1024 mesh points. Since for $a \simeq L$ the instability is extremely slow, we start from $a_0 = 0.1L$. This is a good compromise for limiting computational time while retaining a sufficient dynamical range for the collapse.

4. RESULTS

In Table 1 we list the background and main dynamical parameters for each run, and in Fig. 1 we show for reference the temporal evolution of some unstable Fourier modes of the flux function $\psi_k(y)$, in $y = 0$, from run 2. The growth rate and wave number of the fastest growing mode of the primary tearing at the critical IT threshold will be labelled γ_i and k_i , respectively. In particular, in our simulations we find $k_i L = 10$ and $\gamma_i \tau_A = 0.46$, in agreement with theory (Tenerani et al. 2015).

4.1. Linear stage

Tearing onset takes place at time τ_* , which is well estimated by the condition $\gamma_m(\tau_*)\tau_c = 1$, where $\gamma_m = 0.46 S^{-1/2} (a/L)^{-3/2}$. After onset, the most unstable modes grow according to the WKB solution $\psi_m(t) \sim \exp[\int^t \gamma_m(t') dt']$, represented by the dashed line in Fig. 1. In runs 1–3 we consider different cases of collapse in which $a_\infty/L = S^{-1/3}$. In all these runs the linear stage is ultimately dominated by modes close to the ideally unstable one $k_i L = 10$. Run 4 forces a collapse of the initial sheet down to $a_\infty/L = S^{-1/2}$, but proves that inverse aspect ratios $a/L \ll S^{-1/3}$ cannot be formed:

the tearing mode indeed ignites right after $t = 2.4\tau_A$, at which $a/L = S^{-1/3}$, and a large number of islands rapidly pop up. Even at the end of the linear stage the collapsing sheet thickness is twice the corresponding SP thickness at the given S and P Tenerani et al. (2015).

4.2. Early nonlinear stage

Nonlinearity becomes important at τ_{nl} , when the width w of magnetic islands is of the order of the width of the inner diffusion layer δ . The fastest growing mode has δ_m which scales with the aspect ratio as $\delta_m/a \sim S^{-1/4}(L/a)^{1/4}$. By using the definition $w/a \simeq 2\sqrt{\psi_m/a}$ (Biskamp 2000), we estimate the amplitude $\psi_m(\tau_{nl}) \simeq 0.5 S^{-1/2} [a(\tau_{nl})/L]^{1/2} \simeq 5 \times 10^{-5}$, in agreement with simulations. Nonlinear effects lead to the competition of two processes (Malara et al. 1991): on the one hand, islands start to merge through an inverse cascade process from the fastest growing modes to smaller wave numbers, see, e.g., the inverse cascade from $k_i L = 10$ towards $kL = 5$ and below starting at $\tau_{nl} = 22\tau_A$ (Fig. 1); on the other hand, X-point collapse, and subsequent secondary current sheet formation, takes place during the further nonlinear growth of the islands, as is typical for strongly unstable modes far from the small Δ' regime (Jemella et al. 2003), in lieu of the slow, algebraic Rutherford growth (Rutherford 1973).

4.3. Nonlinear fast tearing cascade

We analyze the fully nonlinear stage using run 1 as a reference, shown in Fig. 2. X-point collapse proceeds leading to the formation of secondary plasmoids (magnetic islands) (Loureiro et al. 2005; Lapenta 2008) and, next, a recursive process of super-Alfvénic secondary layer formation and disruption takes place (Shibata & Tanuma 2001; Daughton et al. 2009). Fig. 2 shows a temporal sequence of recursive plasmoid formation, taking place at the center, near the flow stagnation point of the original instability. Previously, such recursive reconnection has been modeled as a succession of unstable SP layers (Loureiro et al. 2005; Daughton et al. 2009; Uzdensky et al. 2010; Cassak & Drake 2010). Our simu-

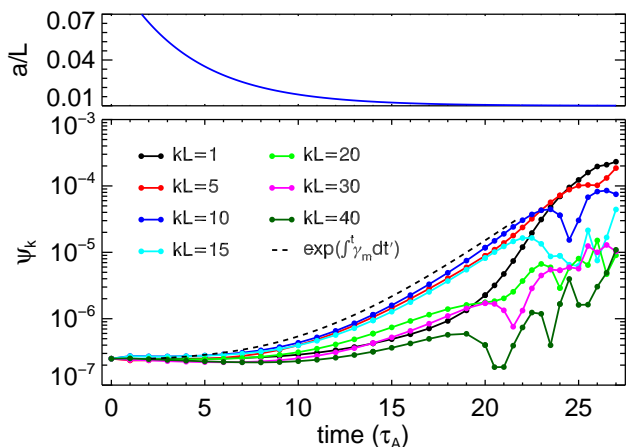


Figure 1. Upper panel: a/L vs. time. Lower panel: temporal evolution of the amplitude of some unstable modes $\psi_k(y)$ at the neutral line $y = 0$ (run 2).

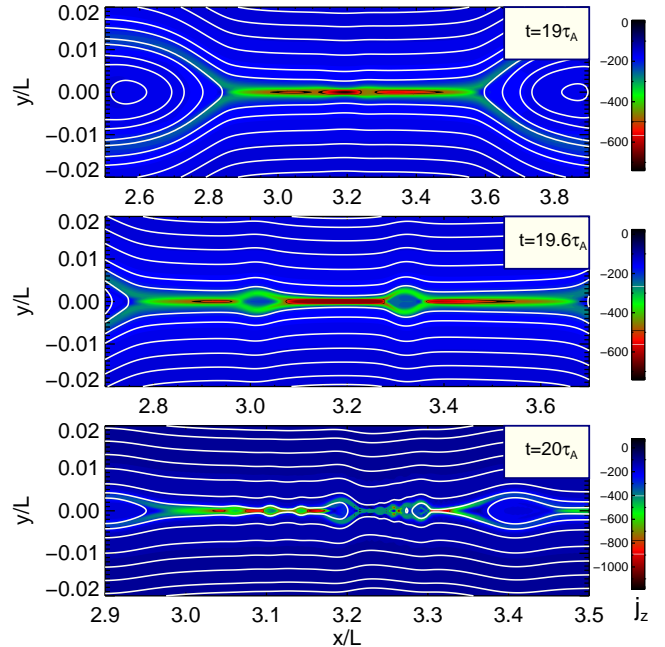


Figure 2. Blow-up of the “ideal” tearing cascade in run 1: contour plot of the out-of-plane current density j_z (color coded) and magnetic field lines (white).

lations show instead that it is driven by onset of the IT mode, triggered by the dynamical *lengthening* of sheets to the local critical threshold, in a way similar to that discussed in section 4.1. As the recursive X-point collapse occurs in steps, we label the half length of the n -th current sheet L_n , the inverse aspect ratio a_n/L_n , the normalized (half) width of the inner diffusion layer δ_n/L_n , the local Lundquist number $S_n = L_n/LS$ and Alfvén time $\tau_{A,n} = L_n/L\tau_A$. Referring to Fig. 2, the cascade starts with the formation of L_1 from the primary inner diffusion region δ_i , hence $a_1 \simeq \delta_i$. Current sheet L_1 becomes unstable, less than $3\tau_A$ after the end of the linear stage (first panel), consistently with what has been observed in (Landi et al. 2015). IT triggering within L_1 induces the growth of two plasmoids and of a second current L_2 , with $a_2 \simeq \delta_1$ (second panel), which is itself destroyed by multiple plasmoids in about $0.5\tau_A$ (third panel). In Fig. 3 we plot the eigenfunctions $B_y(y, x_0)$, in $x_0/L = 3.2$, at three different times, showing the hierarchical structure of IT within each of the inner diffusion layers. To further analyze the tearing onset inside such secondary layers, in Fig. 4, upper panel, we display L_1/L (in green) and a_1/L_1 (in blue) as a function of time, from $t = 15\tau_A$, up to $t = 19\tau_A$. During the collapse process the width remains almost constant, $a_1 \simeq \delta_i \sim LS^{-1/2}$ (here $\delta_i \simeq 0.0015$), while the length L_1 stretches at about a rate $\dot{L}_1/L_1 \simeq \tau_A/\tau_{c,1}$, $\tau_{c,1} \simeq 2\tau_A$. Fig. 4 shows that a_1/L_1 crosses the critical threshold $S_1^{-1/3}$ (red dotted line) at $t \simeq 16\tau_A$. At that time $L_1 \simeq 0.1L$, thus $S_1 \simeq 10^{-5}$, $P = 1$, and linear theory predicts $\gamma_{i,1}\tau_{A,1} \simeq 0.47$, or $\gamma_{i,1}\tau_A \simeq 2.3 \gg \tau_{c,1}^{-1}\tau_A$. In the light of the previous discussion, we would expect L_1 to disrupt more rapidly than in $\simeq 3\tau_A$, though on the same order of magnitude timescale. On the other hand, there is a stabilizing effect from outflows forming along L_1 (Bulanov et al. 1978): these may

induce the formation of thinner sheets having inverse aspect ratio $a_n/L_n \sim S_n^{-\alpha_c}$, with $\alpha_c > 1/3$. Based on the empirical observation that flows stabilize SP up to $S_c \simeq 10^4$, one can generalize the argument to obtain a critical α_c for the IT instability of current sheets with inflow-outflows (Velli et al. 2015):

$$\alpha_c = \frac{2 \log \mu + \log S_n}{3 \log S_n}. \quad (5)$$

In eq. (5), $\mu = \Gamma_v/(f\gamma_i)$ is the ratio of the plasmoid evacuation rate to the maximum growth rate, corrected by a threshold factor $f \simeq 0.5 - 0.1$. The value $\mu = 10$ (Biskamp 2000) yields the observed $\alpha_c = 1/2$ for $S_n = 10^4$, while as expected $\lim_{S_n \rightarrow \infty} \alpha_c = 1/3$. Note that, as shown below, S_n is a decreasing function of n . The black dotted and dash-dotted lines in Fig. 4 (up), correspond to $S_1^{-\alpha_c}$ at two different μ , while the light blue dotted line corresponds to $a_{SP,1}/L_1$. Though our Lundquist numbers are not extremely large, L_1 still disrupts before reaching the SP width. The trend of the data plotted in Fig. 4 goes in the direction of our scenario, that is, that the fast tearing instability is triggered within collapsing current sheets once the critical threshold is reached. Taking into account the increased Alfvén speed due to pile-up just outside the inner diffusion region as considered by (Cassak & Drake 2010) does not change our results. The super-Alfvénic cascade favors an efficient transport of energy to smaller scales, as shown in Fig. 4, lower panel, by the 1D spectra of ψ along the sheet. The slope appears to remain only slightly steeper than a simple power law $\sim k^{-7/5}$ (approached at $kL > 10$) shown in black. This value may be obtained by assuming that the nonlinear amplitude of the flux function saturates at step n with corresponding wave number k_n , when $w_n \simeq \delta_n$, where w_n and δ_n are the n -th island width and width of the inner diffusion layer of the fastest growing mode, respectively: $\psi_n/(B_0 L_n) = 0.5 S_n^{-1/2} (a_n/L_n)^{1/2}$. Assuming IT at step n , $a_n/L_n \sim S_n^{-1/3}$, yields, in our units, $\psi_n = 0.5 (L_n/L)^{1/3} S_n^{-2/3}$. Since the fastest growing mode within L_n is $k_n L_n \sim S_n^{1/6}$, we can write

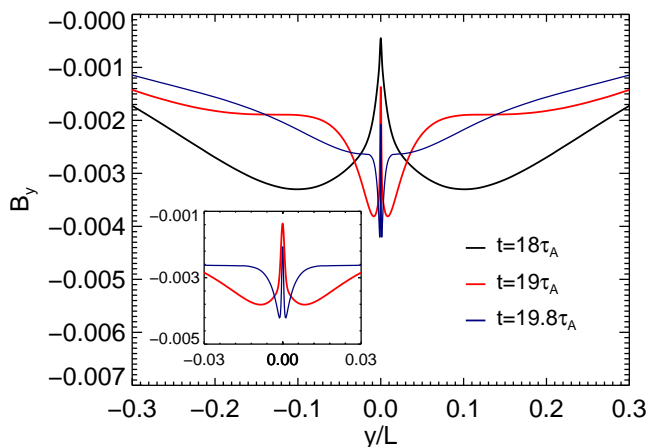


Figure 3. Eigenfunctions of the self-similar hierarchy of “ideal” tearing modes (run 1): plot of $B_y(y, x_0)$ in $x_0/L = 3.2$ at $t = 18 \tau_A$ (primary tearing, $n = 0$), $t = 19 \tau_A$ ($n = 1$), and $t = 19.8 \tau_A$ ($n = 2$).

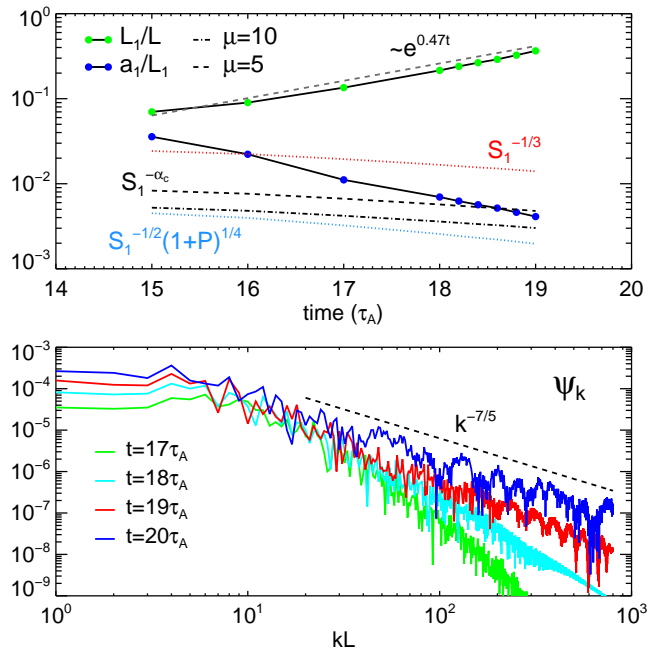


Figure 4. Upper panel: length L_1/L (green) and inverse aspect ratio a_1/L_1 (blue) of the first secondary current sheet vs. time (run 1). The red dotted line represents the critical threshold $S^{-1/3}$, and the light blue dotted line the viscous a_{SP}/L . Black dotted and dash-dotted lines represent the critical threshold with outflow effects, given by eq. (5). Lower panel: 1D spectrum of the flux function, $\psi_k(y)$, in $y = 0$ at four different times during the nonlinear stage (run 1).

$L_n/L = (k_n L)^{-6/5} S^{1/5}$. Finally, expressing the nonlinear amplitude of ψ_n in terms of k_n and going to the continuous limit we obtain:

$$\psi(k) \sim S^{-3/5} (kL)^{-7/5}. \quad (6)$$

The slightly steeper slope observed might be due to the stabilizing outflow effects discussed above.

5. DISCUSSION

We have shown that a collapsing current sheet disrupts due to the triggering of fast reconnection as predicted by the IT model. This process is shown to proceed in a self-similar way giving rise to a hierarchy of fast tearing instabilities at ever smaller scales. Let us model the self-similar collapse of X-points, in the spirit of the original fractal reconnection model, with the following differences: first, we don’t consider SP as the initial condition; second, we use the width a_n , derived from the IT scalings, to find L_n . Neglecting for simplicity viscous and outflow effects, imposing that $a_n/L_{n-1} \sim S_{n-1}^{-1/2}$ (i.e., $a_n \simeq \delta_{n-1}$), and that IT onset occurs at $a_n/L_n \sim S_n^{-1/3}$, we find:

$$L_n = L S^{-1+(3/4)^n}, \quad \tau_{A,n} = L_n \tau_A, \quad S_n = S^{(3/4)^n}. \quad (7)$$

For $n \rightarrow \infty$ then $\tau_{A,n} \rightarrow \tau_A S^{-1}$, and, as expected, $S_n \rightarrow 1$ and $a_n/L_n \rightarrow 1$. However, after a number n_* of steps $S_{n_*} \simeq 10^4$, at which we expect to reach a stable SP. For $S = 10^{13}$ (solar corona) $n_* \simeq 4$, and the length L_n suddenly drops to microscopic scales, $L_1/L \simeq 6 \times 10^{-4}$, $L_2/L \simeq 2 \times 10^{-6}$, $L_3/L \simeq 3 \times 10^{-8}$, $L_4/L \simeq 10^{-9}$. The

cascade after the first trigger thus lasts a time interval $\tau_{tot} \simeq \sum_{n=1}^{n_*} \tau_{A,n} \simeq 5 \times 10^{-4} \tau_A$, one order of magnitude less than the upper limit given by (Shibata & Tanuma 2001). Higher resolution simulations are nevertheless necessary to assess how the cascade saturates. Our scenario can be modified to include kinetic scales which might be reached dynamically in typical astrophysical systems (Cassak et al. 2005; Daughton et al. 2009). In this case we expect a change of the power laws (7) as different scalings describe the physics at the critical threshold in the kinetic regime (Del Sarto et al. 2015).

REFERENCES

- Biskamp, D., 2000, *Magnetic Reconnection in Plasmas* (Cambridge University Press, England)
- Bulanov, S. V. , Syrovatskiĭ, S. I., & Sakai, J. 1978, *JETP* 28, 177
- Cassak, P. A., Shay, M. A., & Drake, J. F. 2005 *Phys. Rev. Lett.*, 95 235002
- Cassak, P. A., & Drake, J. F. 2009, *ApJ* 707, L158
- Cassak, P. A. & Drake, J. F. 2013, *Phys. Plasmas* 20, 061207
- Coppi, B., Pellat, R., Rosenbluth, M., & Galvao, R. 1976, *Soviet Journal of Plasma Physics*, 2, 533
- Daughton, W., Roytershteyn, V., Albright, B. J., Karimabadi, H., et al. 2009, *Phys. Rev. Lett.* 103, 0065004
- Del Sarto, D., Pucci, F. , Tenerani A., & Velli, M. 2015, to be submitted
- Furth, H. P., Killeen, J., & Rosenbluth, M. N. 1963, *Phys. Fluids* 20, 459
- Jemella, B. D., Shay, M. A., & Drake, J. F., 2003, *Phys. Rev. Lett.* 91, 125002
- Landi, S., Velli, M., & Einaudi, L. 2005, *ApJ* 624, 392
- Landi, S., Del Zanna, L., Papini, E. , Pucci, F., et al. 2015, 806, 131
- Lapenta, G. 2008, *Phys. Rev. Lett.* 100, 235001
- Loureiro, N. F., Cowley, S. C., Dorland, W. D., Haines, M. G., et al. 2005, *Phys. Rev. Lett.* 95, 235003
- Loureiro, N. F. , Schekochihin, A. A., & Uzdensky, D. A. 2013, *Phys. Rev. E* 879, 013102
- Malara, F., Veltri, P., & Carbone, V. 1991, *Phys. Fluids B* 3, 1801
- Pucci, F. & Velli, M. 2014, *ApJL*, 780, L19
- Rappazzo, A.F., & Parker, E. N. 2013, *ApJL*, 773, L2
- Rutherford, P. H. 1973, *Phys. Fluids* 16, 1903
- Shibata, K., & Tanuma, S. 2001, *Earth Planets Space* 53 473
- Tenerani, A., Rappazzo, A. F., Velli M., & Pucci, F. 2015, *ApJ* 801, 145
- Uzdensky, D. A., Loureiro, N. F., & Schekochihin, A. A. 2010, *Phys.Rev. Lett.* 105 235002
- Uzdensky, D. A., & Loureiro, N. F. 2014, arXiv:1411.4295
- Velli, M., Matthaeus, W. H., Pucci, F., & Wan, M. 2015 to be submitted
- Velli, M., Pucci, F., Rappazzo, A. F., & Tenerani, A., 2015, *Phil. Trans. R. Soc. A* 373, 20140262